



Geotechnical Testing Journal

A. V. Garcia,¹ R. M. Rached,² and J. C. Santamarina³

DOI: 10.1520/GTJ20170144

Large-Scale True Triaxial Apparatus for
Geophysical Studies in Fractured Rock

TECHNICAL NOTE

A. V. Garcia,¹ R. M. Rached,² and J. C. Santamarina³

Large-Scale True Triaxial Apparatus for Geophysical Studies in Fractured Rock

Reference

Garcia, A. V., Rached, R. M., and Santamarina, J. C., "Large-Scale True Triaxial Apparatus for Geophysical Studies in Fractured Rock," *Geotechnical Testing Journal* <https://doi.org/10.1520/GTJ20170144>. ISSN 0149-6115

ABSTRACT

The study of fractured rock masses in the laboratory remains challenging because of the large specimen sizes and bulky loading systems that are required. This article presents the design, structural analysis, and operation of a compact and self-reacting true triaxial device for fractured rock. The frame subjects a 50 cm by 50 cm by 50 cm fractured rock specimen to a maximum stress of 3 MPa along three independent axes. Concurrent measurements include long-wavelength P-wave propagation, passive acoustic emission monitoring, deformations, and thermal measurements. The device can accommodate diverse research, from rock mass properties and geophysical fractured rock characterizations, to coupled hydro-chemo-thermo-mechanical processes, drilling, and grouting. Preliminary wave propagation data gathered under isotropic and anisotropic stress conditions for an assembly of 4,000 rock blocks demonstrate the system's versatility and provide unprecedented information related to long-wavelength propagation in fractured rock under various stress anisotropies.

Keywords

geophysics, rock mechanics, hydraulic fracturing, true triaxial, fractured rock, jointed rock, rock testing, fracture network, p-wave, load frame

Introduction

The engineering properties of fractured rock masses determine the analysis and engineering design of geosystems such as infrastructure, transportation tunnels, mining, groundwater management, waste storage, and resource recovery ([National Academy of Sciences 2015](#)).

True triaxial devices allow for the study of geomaterials under anisotropic stress conditions, including the effect of the intermediate stress. **Table 1** lists large-scale true triaxial devices for rock testing reported in the literature over the past 50 years. Most devices are for small specimens. In fact, there is an overall inverse relationship between the specimen size and the maximum stress. Furthermore, our analyses show

Manuscript received April 25, 2017; accepted for publication November 1, 2017; published online May 16, 2018.

¹ 4700 King Abdullah University of Science and Technology (KAUST), H4113A-201, Thuwal 23955-6900, Kingdom of Saudi Arabia (Corresponding author), e-mail: adrian.garcia@kaust.edu.sa, <https://orcid.org/0000-0001-7203-6510>

² 4700 King Abdullah University of Science and Technology (KAUST), H4113A-201, Thuwal 23955-6900, Kingdom of Saudi Arabia

³ 4700 King Abdullah University of Science and Technology (KAUST), I559M, Thuwal 23955-6900, Kingdom of Saudi Arabia

TABLE 1 Large-scale true triaxial devices for rock testing reported in the literature (1973–2016).

Size, cm	Stress Level, MPa	Pore Fluid Control	Boundary Control	Reference
60 by 60 by 130	$\sigma_1 = 13.8, \sigma_2 = \sigma_3 = 12$	No	Rubber membranes	Reik and Zacas (1978)
62 by 62 by 120	$\sigma_1 = 15, \sigma_2 = 6, \sigma_3 = 2$	No	Prismatic rubber coating	Natau et al. (1995)
50 by 50 by 50	$\sigma_1 = 40, \sigma_2 = \sigma_3 = 20$	Yes, up to 10 MPa	Silicone grease covered Teflon sheets	Suzuki (2012)
50 by 50 by 50	$\sigma_1 = \sigma_2 = \sigma_3 = 70$	Yes	–	Sibai, Henry, and Gros (1997)
25 by 25 by 25	$\sigma_1 = \sigma_2 = \sigma_3 = 1.5$	Yes	Rubber diaphragm	Ismail, Sharma, and Fahey (2005)
15 by 15 by 15	$\sigma_1 = 44, \sigma_2 = \sigma_3 = 15$	No	Vacuum grease covered polytetrafluoroethylene (PTFE) sheets	Rao and Tiwari (2008)
10 by 10 by 10	$\sigma_1 = 130, \sigma_2 = 60, \sigma_3 = 60$		PTFE sheets	Gau, Cheng, and Zhuo (1983)
10 by 10 by 10	$\sigma_1 = \sigma_2 = \sigma_3 = 65$	No	Flexible polyurethane membranes	Atkinson and Ko (1973)
15 by 6 by 3	$\sigma_1 = 50, \sigma_2 = 60, \sigma_3 = 30$	No	–	He, Miao, and Feng (2010)
10 by 5 by 5	$\sigma_1 = \sigma_2 = 1,000, \sigma_3 = 100$	Yes	Copper foil and TFE-fluorocarbon or PTFE sheets with grease	Shi et al. (2017)
10 by 5 by 5	$\sigma_1 = 1,000, \sigma_2 = 200, \sigma_3 = 200$	No	Two greased copper sheets	Michelis (1985)

that the cost of large-scale triaxial devices increases nonlinearly with the specimen size and operating stress range.

The study and characterization of fractured rock masses in the laboratory under a three-dimensional state of stress necessitates the use of large-scale loading devices to attain effective media conditions. This is particularly the case for geophysical characterization: long-wavelength propagation studies require that the wavelength λ is much larger than the fracture spacing b ($\lambda > 10b$, Brillouin 1946). Previous laboratory studies have focused on wave propagation across multiple fractures in the short-wavelength regime (Sjogren, Øfsthus, and Sandberg 1979; El-Naqa 1996; Kahraman 2001; Kurtuluş et al. 2012) or ballistic propagation across a single, isolated fracture (Pyrak-Nolte, Myer, and Cook 1990; Pyrak-Nolte, Xu, and Haley 1992; Zhao and Cai 2001). Studies that satisfied long-wavelength propagation conditions only explored a one-dimensional geometric configuration (Fratta and Santamarina 2002; Cha, Cho, and Santamarina 2009; Mohd-Nordin et al. 2014).

This article presents the design and operation of a large-scale true triaxial rock testing device developed at King Abdullah University of Science and Technology (KAUST) for the characterization of fractured rock specimens and the study of coupled processes in fractured rocks under isotropic and deviatoric stress-controlled conditions. Then, long-wavelength P-wave measurements across a specimen made of precut limestone blocks are used to demonstrate the versatility of the true triaxial frame.

KAUST True Triaxial Device for Fractured Rock

The design objectives of the true triaxial frame are as follows: (1) subject a prefractured rock specimen to boundary stresses up to $\sigma' = 3$ MPa; (2) independently control the three principal stresses imposed at the boundaries; (3) mitigate the side friction

and corner effects on the stress field; and (4) allow for extensive instrumentation and monitoring under preselected stress paths. Note that the system was not designed for stress–strain studies of fractured rocks.

The specimen dimensions are 50 cm by 50 cm by 50 cm. This size readily accommodates various fracture topologies and allows for effective media studies when blocks several centimeters in size form the fractured rock.

Thin hydraulic flat jacks 50 cm by 50 cm by 0.4 cm mounted on the six faces of the cubical specimen control the principal stresses (Fig. 1a). A 3-mm-thick rubber layer sits between the flat jacks and the rock mass; this layer reduces the accumulation of friction along transverse boundaries and favors a more homogeneous normal stress distribution against the fractured rock mass. We use aluminum plates 50 cm by 50 cm as spacers between the flat jacks and the rubber layer to fill the gap between the jacks and the specimen for different fabric configurations. Finally, the flat jacks rest against the thick reaction plates mounted on the frame.

The selected 2.5 cm by 2.5 cm by 5 cm rock blocks rest at the corners between the normal flat jacks. Then, a 1-cm corner gap between neighboring flat jacks prevents corner effects. This small gap is possible because of the low compressibility of rock masses (Fig. 1b).

FRAME DESIGN

Fig. 2 presents the exploded view of the essential components of the true triaxial frame (details in Table 2). Measured from the outside edges, the total size of the device is 112 cm by 112 cm by 112 cm. The internal dimensions account for the cubic specimen, the added thickness of the hydraulic flat jacks, and the stiff reaction plates. A single-piece square frame rests horizontally to resist horizontal forces in the x- and y-directions. The top and bottom H-shaped structures are bolted onto the horizontal frame to complete the cube. We use a hand-operated gantry crane to remove the top structure and gain access to the specimen.

FIG. 1 (a) Boundary assembly and (b) corner gap details. Components: (1) fractured rock specimen, (2) thin piezoelectric element and other flat sensors, (3) rubber sheet, (4) aluminum plate spacers (as needed), (5) flat jack, (6) steel reaction plate and (7) steel I-beam frame.

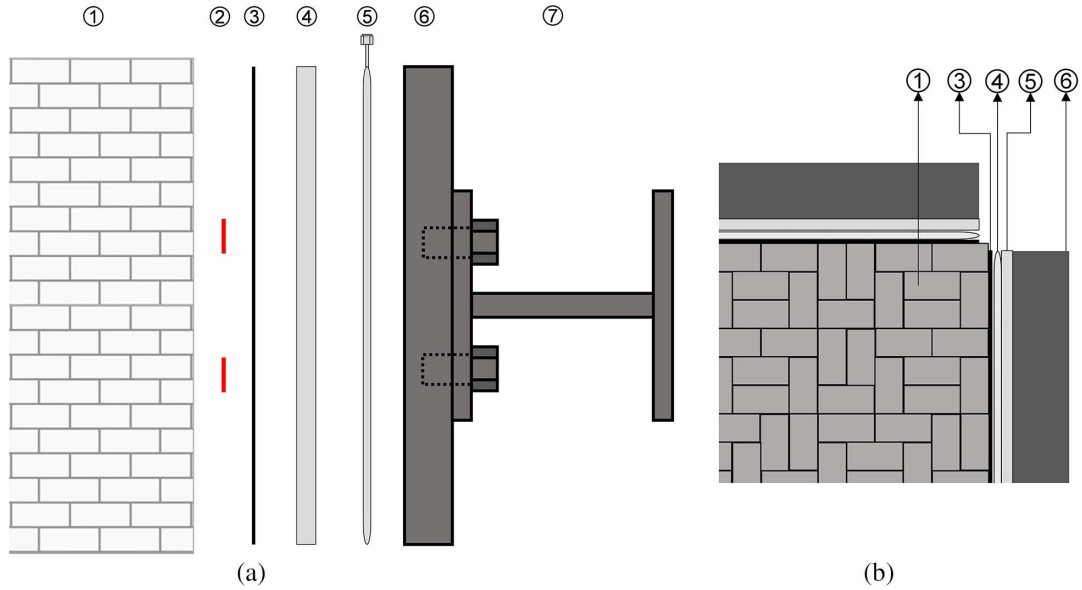


FIG. 2 Reaction frame: finite element simulation results. von Mises stress distribution when the frame imposes a 3 MPa loading on an internal specimen. Component numbers: refer to **Table 2** for details.

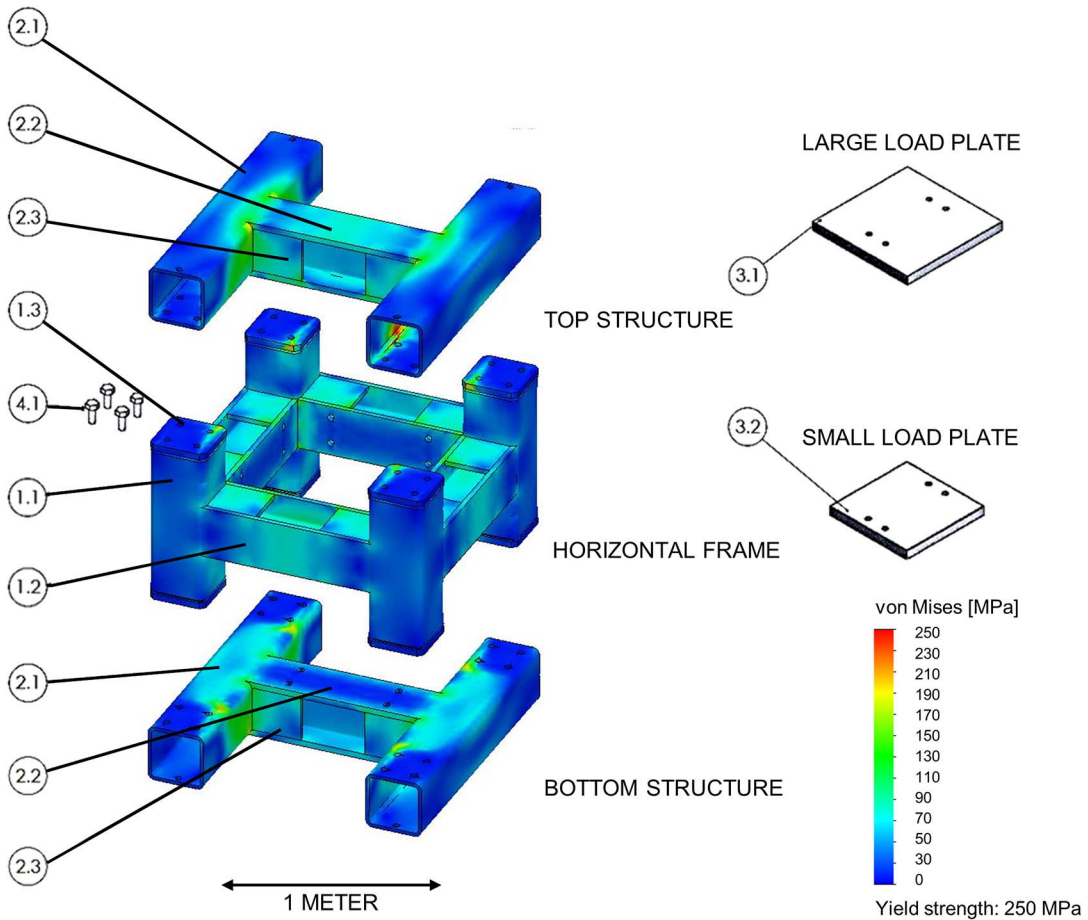


TABLE 2 Steel frame design geometric details (refer to Fig. 2).

Element	Part Name	Description	Quantity	Item # in Fig. 2 ^a
Midsquare frame	Tube Caps	230 by 230 by 25 mm	8	1.1
	Tube Columns	230 by 230 by 14 by 619 mm	4	1.2
	Middle I-Beams	210 by 210 by 14 by 664 mm	4	1.3
Top and bottom H-sections	Tube Beam	230 by 230 by 1,120 mm	4	2.1
	Middle I-Beam	210 by 210 by 14 by 664 mm	2	2.2
	Shear Stiffener	660 by 180 by 13 mm	12	2.3
Load plates	Small Load Plate	510 by 510 by 50 mm	5	3.1
	Large Load Plate	630 by 630 by 50 mm	1	3.2
Peripherals	Bolts	M27	56	4.1

Note: ^aItems 1.1 through 3.2 are ASTM A36, Standard Specification for Carbon Structural Steel, steel, while item 4.1 is ASTM A325, Standard Specification for Structural Bolts, Steel, Heat Treated, 120/105 ksi Minimum Tensile Strength (withdrawn 2016), steel.

STRUCTURAL ANALYSIS OF THE CUBICAL FRAME

The target maximum operational load is $\sigma' = 3$ MPa in each direction. The critical design constraints are the bending and shear of the central I-beams on all six sides, pull-out failure of the welded tube caps, and shear/tensile failure of the bolts. Fig. 2 presents the von Mises stress field for the main frame components under a homogeneous 3 MPa distributed load on all six load plates (SolidWorks 2015, Young’s Modulus $E = 2 \times 10^{11}$ N/m², Poisson’s ratio $\nu = 0.26$, mass density $\rho = 7,850$ kg/m³, tensile strength $\sigma_t = 400$ MPa, and yield strength $\sigma_y = 250$ MPa). The analysis shows that no frame components yield. The webs of the I-beams experience the highest stresses; the stiffeners welded on all the I-beams contribute shear strength at the beam connections.

Fig. 3 shows the measured and calculated load-deformation frame response in the vertical and horizontal directions for isotropic loading. The as-built flexural rigidity EI used in the finite element method simulation is 30 % greater than the nominal value reported by the manufacturers of the I-beams. Measured

and predicted load-deformation trends are linear for the 1 MPa stress imposed in this test. Nonlinearity becomes apparent in numerical simulations when $\sigma_0 \geq 3.5$ MPa. The displacement at $\sigma_0 = 1$ MPa reaches $\delta_z = 0.45$ mm in the vertical direction but is only $\delta_x = \delta_y = 0.12$ mm in the horizontal x- and y-directions because of the stiffer single-piece horizontal frame (refer to Fig. 2). The frame’s deformation does not affect the imposed stress field: the flexible flat jacks exert a near-uniform stress distribution on the specimen faces.

LOADING SYSTEM

The steel flat jacks mounted on all six sides can withstand 10 MPa of internal pressure. They are very compliant: the measured unsupported stiffness is ~ 3 kPa/mm. Each flat jack pair in the x-, y- and z-directions is connected to an independent syringe pump as shown in Fig. 4a (Isco 1000D filled with hydraulic oil [Teledyne Isco Inc., Lincoln, NE]). The syringe pumps can operate in either flow-rate or pressure-control modes. A LabVIEW-based software

FIG. 3

Measured (dots) and finite element computed (lines) stress-deformation trends for the frame during isotropic loading.

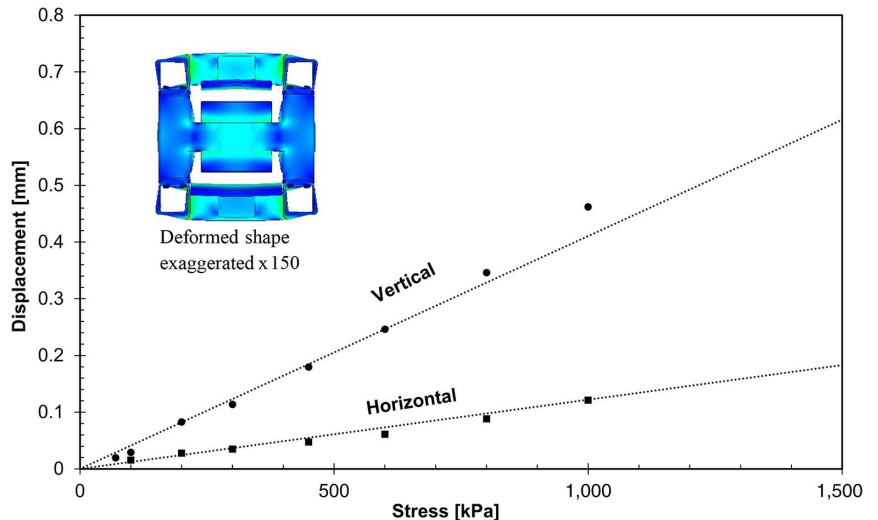
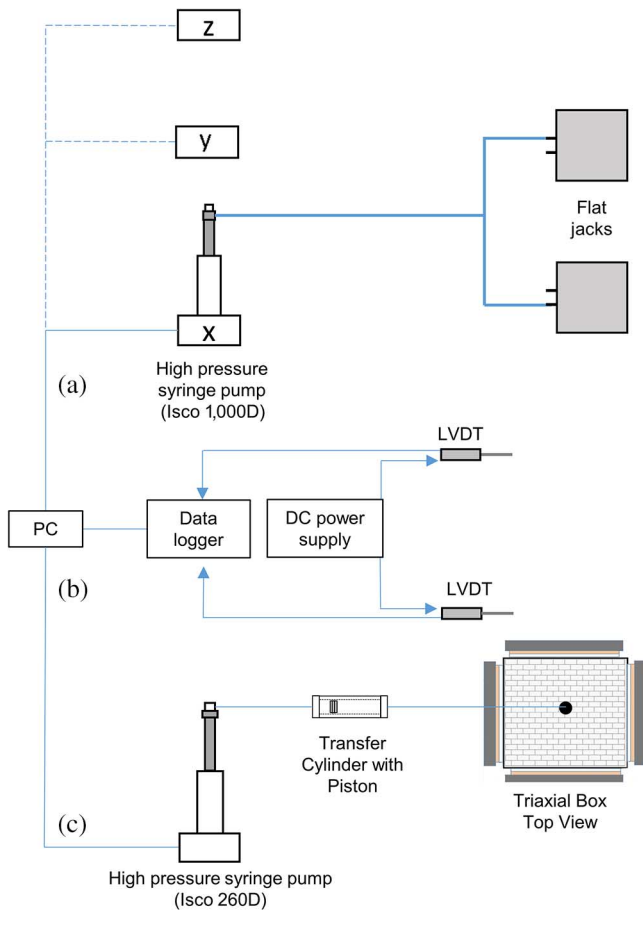


FIG. 4 Control and monitoring: (a) pressure-volume control, (b) sensor data acquisition (LVDT = linear variable differential transducers), and (c) additional fluid injection system.



(National Instruments, Austin, TX) commands the pumps and logs pump data at preselected time intervals.

There is an additional syringe pump connected to a fluid transfer cylinder to inject high-viscosity fluids into the specimen. This pump allows us to investigate hydro-chemo-mechanical coupled processes in fractured rocks such as the nature of hydraulic fracturing in prefractured media (Fig. 4c).

INSTRUMENTATION

Linear variable differential transducers monitor the external vertical and horizontal deformations of the frame (Fig. 4b). We combine frame deformation and jack inflation monitored with the syringe pumps to obtain a first-order estimate of the specimen deformation.

Long-wavelength propagation studies rely on thin piezoelectric pads (with a diameter of 2.5 cm and a thickness of 1 mm) placed at the center of each face. These P-wave sources and receivers connect to the function generator, filter-amplifier, and a digital oscilloscope that is used for visualization and storage (Fig. 5).

The piezoelectric pads on all six sides of the specimen and eight accelerometers (with frequencies of 2–10 kHz) buried within rock blocks distributed throughout the specimen detect acoustic emissions such as those generated during hydraulic fracturing studies (Fig. 6a and b).

The large specimen size and controlled boundary conditions readily allow for other monitoring systems such as electrical resistivity tomography and thermocouples and point-heaters for thermal diffusion/conduction studies.

Test Protocol—Demonstration

Specimen preparation is critical to the study of fractured rocks in the laboratory, particularly when effective media behavior is sought (e.g., long-wavelength propagation studies), because a large number of blocks are required under true triaxial conditions. Specimen preparation, boundary details, and selected data gathered as part of this study follow.

SPECIMEN PREPARATION—TEST PROCEDURES

We use precut limestone blocks to build the fractured rock mass. The dimensions of each block 2.5 cm by 2.5 cm by 5 cm are selected to allow for long wavelength propagation studies in a wide range of configurations and fabric anisotropies ($\lambda > 10b$, where b is the block size). X-ray diffraction analyses show that the limestone is made of calcite and dolomite. The P-wave velocity through intact blocks is $V_p = 6,300 \pm 200$ m/s and the density is $2,670 \pm 20$ kg/m³.

This manuscript presents data gathered with two fabric configurations: (1) 20 layers with blocks laid horizontally in random

FIG. 5 Seismic signal delivery and acquisition system.

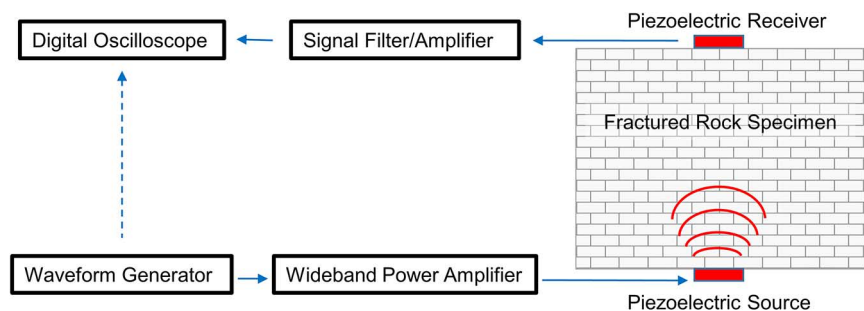
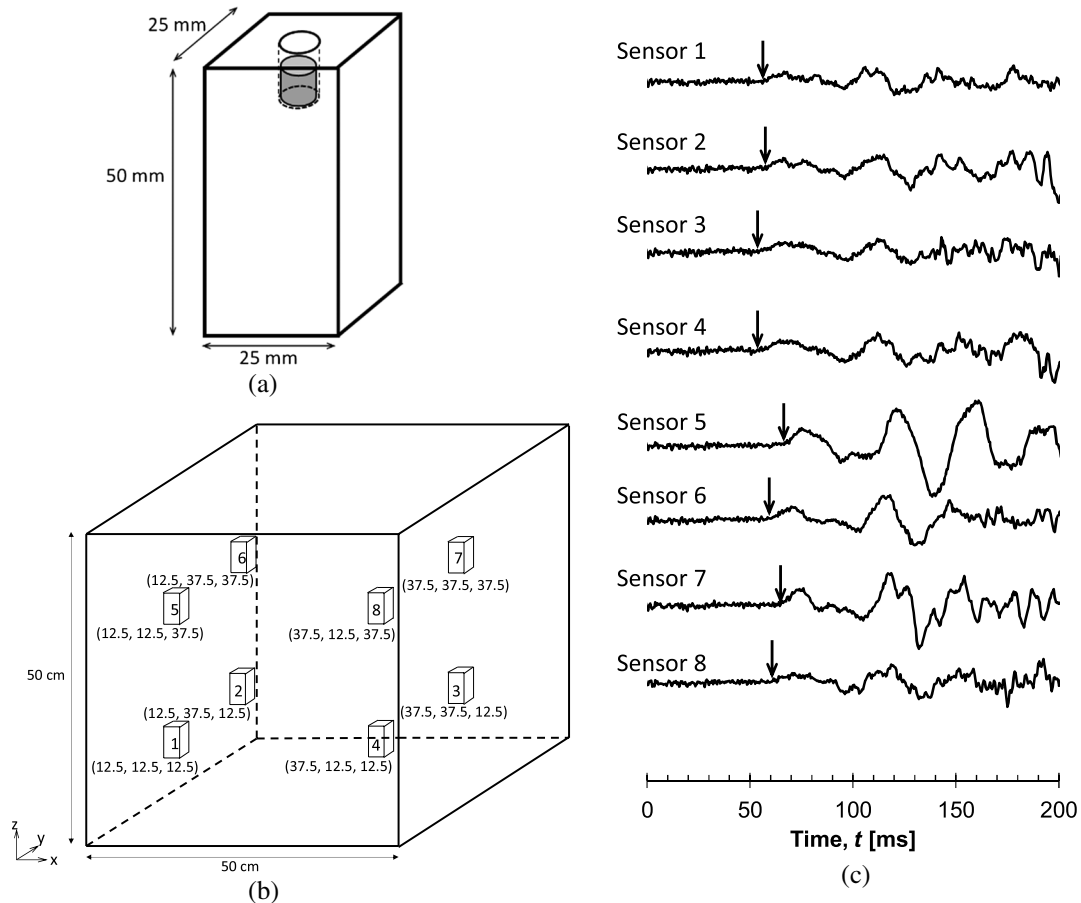


FIG. 6 Passive acoustic emissions. (a) Instrumented blocks with buried accelerometer (PCB 352B10 [PCB Piezotronics, Depew, NY]). (b) Location of installed blocks within the rock mass. (c) Typical acoustic emission event captured during hydraulic fracturing using the eight buried accelerometers. Arrows mark first arrivals.



patterns, and (2) 10 layers arranged in vertical columns. Sketches of both fabric arrangements are shown in Fig. 7. We brush carbonate gouge on every layer to fill openings (passing sieve #40 and retained on sieve #200). The boundary assembly shown in Fig. 1 is used in all tests.

TYPICAL DATA—LONG-WAVELENGTH PROPAGATION

Fig. 7 presents two cascades of P-wave signatures gathered in the x-direction during isotropic loading to $\sigma' = 1$ MPa for two different block configurations. Arrival times vary inversely proportional with the applied stress σ'_x . There is a noticeable shift to higher frequencies as stresses increase because of the following: (1) the stress-dependent piezoelectric response when pads are installed against the specimen and (2) Brillouin low pass filtering in the discrete rock fabrics (Santamarina and Aloufi 1999). These signature cascades have a similar stress response to that reported for soils under true triaxial stress conditions (Stokoe, Lee, and Knox 1985; Ismail, Sharma, and Fahey 2005).

The true triaxial device allows for the independent control of the three principal stresses. Fig. 8 shows the evolution of

long-wavelength P-wave velocities in the three principal stress directions. We initially confine the specimen to an isotropic loading of 100 kPa. This is followed by deviatoric loading in the x-direction to a maximum load of $\sigma'_x = 1,000$ kPa while keeping $\sigma'_y = \sigma'_z = 100$ kPa. The wave velocity in the fractured rock is much lower than that of the intact rock ($V_p = 6,300$ m/s) in all cases. The P-wave velocity increases during loading in the direction of the applied stress, which is similar to the response in silica sand under the same loading conditions (Stokoe, Lee, and Knox 1985); however, unlike the sand, the velocities' responses in the transverse directions are dependent on the deviatoric load (for comparison, see Ismail, Sharma, and Fahey 2005).

The wave propagation velocity in the fractured rock mass is much more sensitive to stress than the intact rock (see also Sayers, Van Munster, and King 1990). All V_p - σ' trends during loading are Hertzian-type power functions $V_p = \alpha(\sigma'/\text{kPa})^\beta$ where the α -factor is the nominal P-wave velocity when $\sigma' = 1$ kPa and the β -exponent reflects the stress sensitivity. The α -factor and β -exponent for fractured rocks tested in this study plot above the α - β trends for all soils reported worldwide are in agreement

FIG. 7

Typical x-direction P-wave cascade dataset for two fracture fabrics.

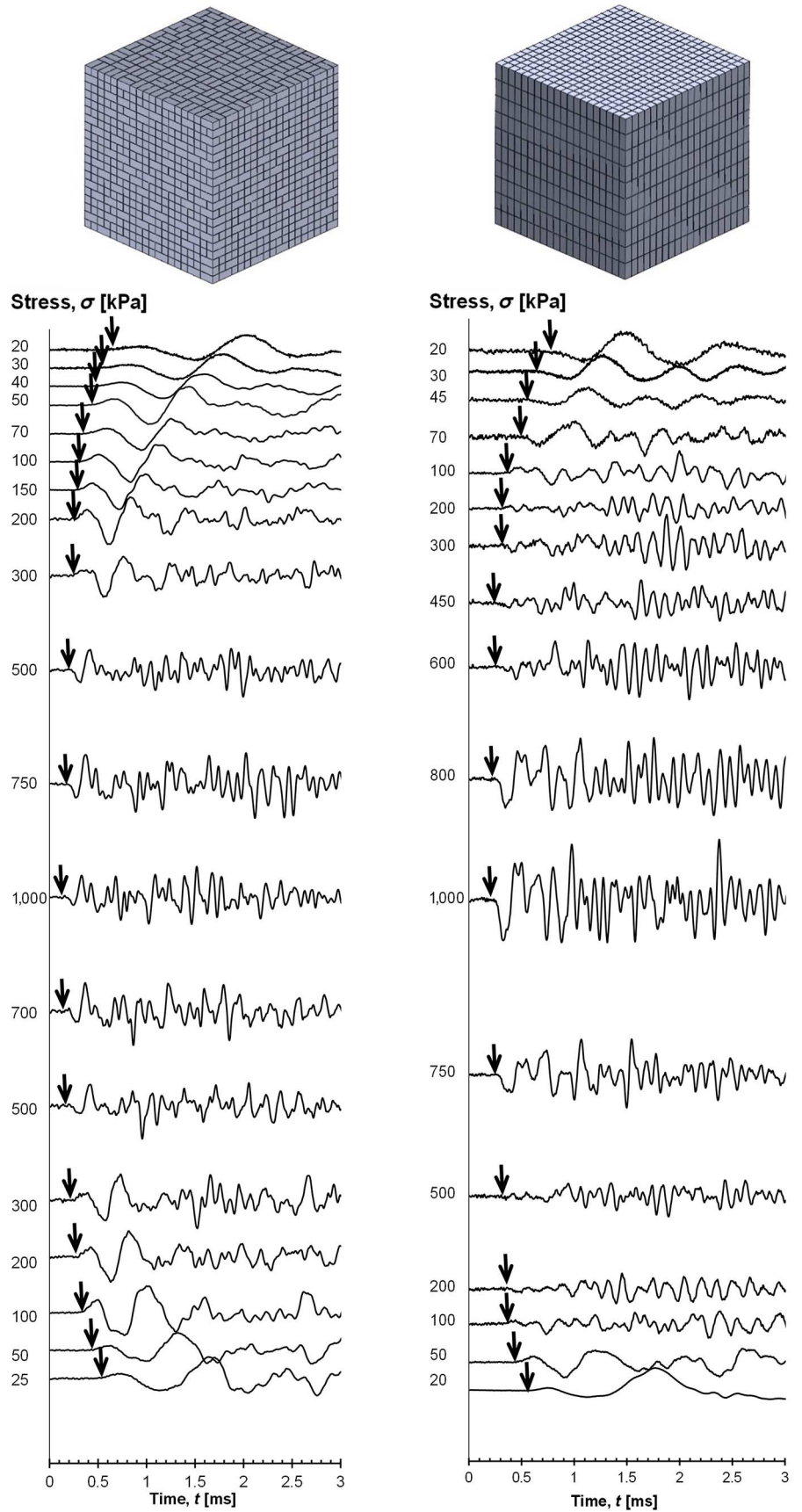
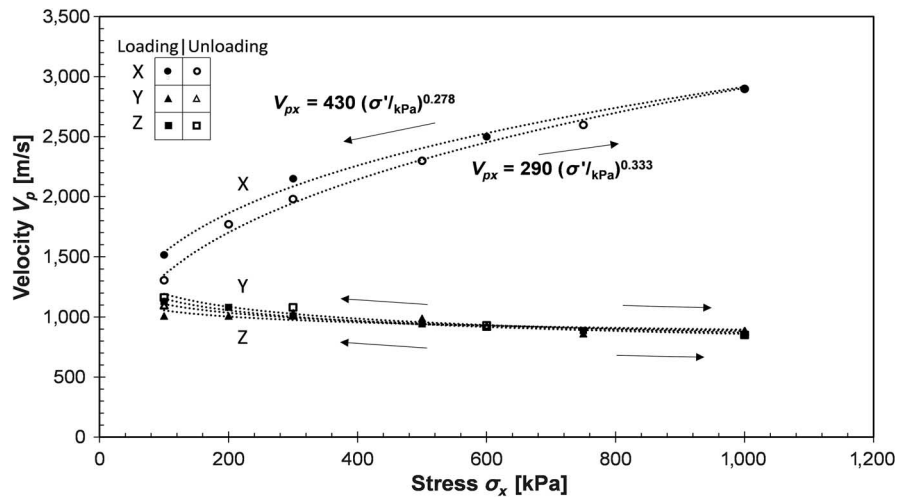


FIG. 8

Evolution of P-wave velocities during deviatoric loading in the x-direction while keeping $\sigma'_y = \sigma'_z = 100$ kPa.



with previously reported one-dimensional data gathered for fractured rock specimens made of stacked blocks (Fratta and Santamarina 2002; Cha, Cho, and Santamarina 2009). This result highlights inherent differences in the stress-dependent stiffness between fractured rocks and soils.

Fig. 6c depicts a typical acoustic-emission dataset gathered during hydraulic fracturing using all eight accelerometers buried within blocks inside the specimen. Arrival times, amplitudes, and signatures allow us to locate the emission source and to infer the source mechanism (Nelson and Glaser 1992; Lockner 1993).

Discussion: Advantages and Shortcomings

The KAUST true triaxial frame for the study of fracture rock masses can accommodate a large number of rock blocks to determine the effective-media, long-wavelength parameters. Regular rock blocks can be arranged in different configurations to explore the role of fabric on physical processes. Alternatively, three-dimensional-printed blocks can be assembled to reproduce any given fractured rock mass of interest.

The loading system enables the independent control of the three principal stresses and allows for repetitive loading and time-dependent studies such as creep. The compliant flat jacks stress the specimen faces with a near-uniform stress distribution.

The cost effective, versatile, and compact frame is based on a self-reactive design. It has readily accessible boundaries that facilitate the installation of instrumentation for active and passive geophysical measurements and for the monitoring of coupled hydro-chemo-thermo-mechanical processes. The frame is easily assembled to facilitate specimen preparation and permits fluid injection into the fractured rock specimen.

The device is designed for relatively low stresses of 3 MPa. Therefore, it is not meant for the study of failure conditions; the data are particularly relevant to near-surface geotechnical engineering applications. Bladder inflation is a proxy measurement of deformation and requires careful correction for frame deformation.

Conclusions

The study of fractured rock under a three-dimensional state-of-stress necessitates the development of large-scale reaction frames. This article described the design and operation of a compact, self-reacting frame that can impose a 3 MPa stress onto a 50 cm by 50 cm by 50 cm fractured rock specimen. Multiple auxiliary systems measure boundary stresses and deformations in all three principal directions, long-wavelength P-wave velocities, acoustic emissions, and thermal phenomena.

Potential engineering applications and implications comprise research into rock mass properties for various fracture topologies and fabrics (alternating stiff/soft layers, three-dimensional printed rock blocks, gouge material), the geophysical characterization of fractured rock (long-wavelength propagation) and heat transfer (geothermal energy and thermally-active foundations), coupled hydro-chemo-thermo-mechanical processes (including hydraulic fracture studies in prefractured rocks under true triaxial stress conditions), repetitive loading, drilling, grouting, and cementation efficiency in fractured rock masses subjected to anisotropic stress fields.

Unprecedented P-wave velocity data gathered under isotropic and anisotropic stress conditions for two different fabrics confirm the pronounced stress-dependency in long-wavelength velocity in fractured rock, show softening in directions normal to loading, and anticipate distinct constitutive model parameters as compared to other granular materials.

ACKNOWLEDGMENTS

Financial support for this research was provided by the KAUST endowment. The authors would like to thank Gabrielle Abelskamp for her assistance with editing this manuscript.

References

- Atkinson, R. and Ko, H.-Y., 1973, "A Fluid Cushion, Multiaxial Cell for Testing Cubical Rock Specimens," *Int. J. Rock Mech. Min. Sci. Geomech. Abstr.*, Vol. 10, No. 4, pp. 351–354, [https://doi.org/10.1016/0148-9062\(73\)90043-0](https://doi.org/10.1016/0148-9062(73)90043-0)
- Brillouin, L., 1946, *Wave Propagation in Periodic Structures: Electric Filters and Crystal Lattices*, Courier Corporation, Mineola, NY, 225p.
- Cha, M., Cho, G.-C., and Santamarina, J. C., 2009, "Long-Wavelength P-Wave and S-Wave Propagation in Jointed Rock Masses," *Geophysics*, Vol. 74, No. 5, pp. E205–E214, <https://doi.org/10.1190/1.3196240>
- El-Naqa, A., 1996, "Assessment of Geomechanical Characterization of a Rock Mass Using a Seismic Geophysical Technique," *Geotech. Geol. Eng.*, Vol. 14, No. 4, pp. 291–305, <https://doi.org/10.1007/BF00421945>
- Fratta, D. and Santamarina, J. C., 2002, "Shear Wave Propagation in Jointed Rock: State of Stress," *Géotechnique*, Vol. 52, No. 7, pp. 495–505, <https://doi.org/10.1680/geot.2002.52.7.495>
- Gau, Q.-Q., Cheng, H.-T., and Zhuo, D.-P., 1983, "The Strength Deformation and Rupture Characteristics of Red Sandstone under Polyaxial Compression," presented at the *Fifth ISRM Congress*, Melbourne, Australia, International Society for Rock Mechanics, Lisbon, Portugal.
- He, M. C., Miao, J. L., and Feng, J. L., 2010, "Rock Burst Process of Limestone and Its Acoustic Emission Characteristics under True-Triaxial Unloading Conditions," *Int. J. Rock Mech. Min. Sci.*, Vol. 47, No. 2, pp. 286–298, <https://doi.org/10.1016/j.ijrmms.2009.09.003>
- Ismail, M., Sharma, S., and Fahey, M., 2005, "A Small True Triaxial Apparatus with Wave Velocity Measurement," *Geotech. Test. J.*, Vol. 28, No. 2, pp. 113–122, <https://doi.org/10.1520/GTJ12648>
- Kahraman, S., 2001, "A Correlation between P-Wave Velocity, Number of Joints and Schmidt Hammer Rebound Number," *Int. J. Rock Mech. Min. Sci.*, Vol. 38, No. 5, pp. 729–733, [https://doi.org/10.1016/S1365-1609\(01\)00034-X](https://doi.org/10.1016/S1365-1609(01)00034-X)
- Kurtuluş, C., Üçkardeş, M., Sarı, U., and Güner, Ş. O., 2012, "Experimental Studies in Wave Propagation across a Jointed Rock Mass," *Bull. Eng. Geol. Environ.*, Vol. 71, No. 2, pp. 231–234, <https://doi.org/10.1007/s10064-011-0392-5>
- Lockner, D., 1993, "The Role of Acoustic Emission in the Study of Rock Fracture," *Int. J. Rock Mech. Min. Sci. Geomech. Abstr.*, Vol. 30, No. 7, pp. 883–899, [https://doi.org/10.1016/0148-9062\(93\)90041-B](https://doi.org/10.1016/0148-9062(93)90041-B)
- Michelis, P., 1985, "A True Triaxial Cell for Low and High Pressure Experiments," *Int. J. Rock Mech. Min. Sci. Geomech. Abstr.*, Vol. 22, No. 3, pp. 183–188, [https://doi.org/10.1016/0148-9062\(85\)93233-4](https://doi.org/10.1016/0148-9062(85)93233-4)
- Mohd-Nordin, M. M., Song, K.-I., Cho, G.-C., and Mohamed, Z., 2014, "Long-Wavelength Elastic Wave Propagation across Naturally Fractured Rock Masses," *Rock Mech. Rock Eng.*, Vol. 47, No. 2, pp. 561–573, <https://doi.org/10.1007/s00603-013-0448-x>
- Natau, O., Fliege, O., Mutschler, T. T., and Stech, H.-J., 1995, "True Triaxial Tests of Prismatic Large Scale Samples of Jointed Rock Masses in Laboratory," presented at the *Eighth ISRM Congress*, Tokyo, Japan, International Society for Rock Mechanics, Lisbon, Portugal.
- National Academy of Sciences, 2015, *Characterization, Modeling, Monitoring, and Remediation of Fractured Rock*, National Academies Press, Washington, DC, 244p.
- Nelson, P. P. and Glaser, S. D., 1992, "Acoustic Emissions Produced by Discrete Fracture in Rock Part 1—Source Location and Orientation Effects," *Int. J. Rock Mech. Min. Sci. Geomech. Abstr.*, Vol. 29, No. 3, pp. 237–251, [https://doi.org/10.1016/0148-9062\(92\)93658-7](https://doi.org/10.1016/0148-9062(92)93658-7)
- Pyrak-Nolte, L. J., Myer, L. R., and Cook, N. G., 1990, "Transmission of Seismic Waves across Single Natural Fractures," *J. Geophys. Res. Solid Earth*, Vol. 95, No. B6, pp. 8617–8638, <https://doi.org/10.1029/JB095iB06p08617>
- Pyrak-Nolte, L. J., Xu, J., and Haley, G. M., 1992, "Elastic Interface Waves Propagating in a Fracture," *Phys. Rev. Lett.*, Vol. 68, No. 24, pp. 3650–3653, <https://doi.org/10.1103/PhysRevLett.68.3650>
- Rao, K. S. and Tiwari, R. P., 2008, "A Polyaxial System for Testing of Jointed Rock Mass Models," *Geotech. Test. J.*, Vol. 31, No. 4, pp. 285–294, <https://doi.org/10.1520/GTJ100768>
- Reik, G. and Zacas, M., 1978, "Strength and Deformation Characteristics of Jointed Media in True Triaxial Compression," *Int. J. Rock Mech. Min. Sci. Geomech. Abstr.*, Vol. 15, No. 6, pp. 295–303, [https://doi.org/10.1016/0148-9062\(78\)91470-5](https://doi.org/10.1016/0148-9062(78)91470-5)
- Santamarina, J. C. and Aloufi, M., 1999, "Small Strain Stiffness: A Micromechanical Experimental Study," presented at the *Second International Symposium on Pre-failure Deformation Characteristics of Geomaterials*, Torino, Italy, CRC Press, Boca Raton, FL, pp. 451–458.
- Sayers, C. M., Van Munster, J. G., and King, M. S., 1990, "Stress-Induced Ultrasonic Anisotropy in Berea Sandstone," *Int. J. Rock Mech. Min. Sci. Geomech. Abstr.*, Vol. 27, No. 5, pp. 429–436, [https://doi.org/10.1016/0148-9062\(90\)92715-Q](https://doi.org/10.1016/0148-9062(90)92715-Q)
- Shi, L., Li, X., Bing, B., Wang, A., Zeng, Z., and He, H., 2017, "A Mogi-Type True Triaxial Testing Apparatus for Rocks with Two Moveable Frames in Horizontal Layout for Providing Orthogonal Loads," *Geotech. Test. J.*, Vol. 40, No. 4, pp. 542–558, <https://doi.org/10.1520/GTJ20160242>
- Sibai, M., Henry, J. P., and Gros, J. C., 1997, "Hydraulic Fracturing Stress Measurement Using a True Triaxial Apparatus," *Int. J. Rock Mech. Min. Sci.*, Vol. 34, Nos. 3–4, pp. 289.e1–289.e210, [https://doi.org/10.1016/S1365-1609\(97\)00058-0](https://doi.org/10.1016/S1365-1609(97)00058-0)
- Sjogren, B., Øfsthus, A., and Sandberg, J., 1979, "Seismic Classification of Rock Mass Qualities," *Geophys. Prospect.*, Vol. 27, No. 2, pp. 409–442, <https://doi.org/10.1111/j.1365-2478.1979.tb00977.x>
- Stokoe, K., Lee, S., and Knox, D., 1985, "Shear Moduli Measurements under True Triaxial Stresses," presented at the *Convention on Advances in the Art of Testing Soils under Cyclic Conditions*, Detroit, MI, American Society of Civil Engineers, pp. 166–185.
- Suzuki, K., 2012, "Study of the Failure and Deformability of Jointed Rock Masses Using Large Rock Block Specimens," *True Triaxial Testing of Rocks*, CRC Press, Boca Raton, FL, pp. 61–70.
- Zhao, J. and Cai, J. G., 2001, "Transmission of Elastic P-Waves across Single Fractures with a Nonlinear Normal Deformational Behavior," *Rock Mech. Rock Eng.*, Vol. 34, No. 1, pp. 3–22, <https://doi.org/10.1007/s006030170023>